J. Fluid Mech. (1989), *vol.* 203, *pp.* 149–171
Printed in Great Britain

Surface-tension effects in the contact of liquid surfaces

By HASAN N. OGUZ AND ANDREA PROSPERETTI
Department of Mechanical Engineering, The John Hopkins University, Baltimore, MD 21218, USA

(Received 8 June 1988 and in revised form 9 November 1988)

The process by which two surfaces of the same liquid establish contact, as when two drops collide or raindrops fall on water, is studied. The mathematical formulation is based on the assumption of an incompressible, inviscid fluid with surface tension. A model problem with a simplified geometry is solved numerically by means of a boundary-integral method. The results imply that a number of toroidal bubbles form and remain entrapped between the contacting surfaces. Experimental evidence for this process, which is important for boiling nucleation and the formation of condensation nuclei for rain drops, is found in the literature.

1. Introduction

We consider the process by which two surfaces of the same liquid come into contact, as for example when two droplets collide or a raindrop falls on water. A number of complex events take place just before and after the contact. Viscous effects become important in the air film separating the surfaces as it thins and they exert a significant stress on the liquid. A very brief stage of free molecular flow follows. Just at the moment at which contact is established the free surface has a cusp at the contact point, which is incompatible with the state of local thermodynamic equilibrium that is assumed to incorporate the effects of surface tension in fluid mechanics. Such a strong disequilibrium cannot persist over the timescales of concern in a classical fluid mechanical description of the process and almost instantly the cusp must be replaced by a region of continuous, if very sharp curvature.

However complex these processes, their total effect on the macroscopic fluid dynamics of the collision cannot be very important for droplets larger than a few microns. For droplets having a radius of the order of 100 μm or greater, one expects that classical fluid mechanics should be amply sufficient to explain the basic features of the collision. In such a framework the configuration with a high curvature just after the disappearance of the cusp can be taken as an initial condition, and the problem we consider in this study is to determine how this region evolves and propagates outwards as the two liquid masses get closer.

When we started this work we qualitatively expected the process to evolve according to a sequence of events that may be illustrated with reference to figure 1. The curvature along the ring AA' is very large and, therefore, the liquid pressure is very small because of the effect of surface tension. This circumstance induces a large outward velocity along this ring. As the liquids approach each other the curvature would seem to increase further and with it the radial velocity in such a way that no further contact between the two facing liquid masses along rings such as BB' and CC'

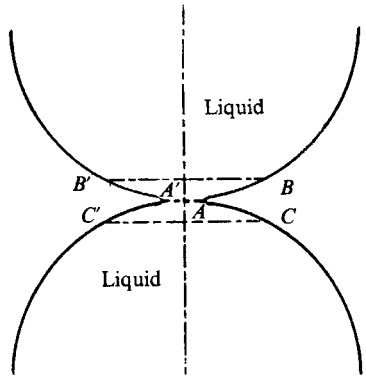

FIGURE 1. The initial moment of the impact of two liquid drops touching at one point where a 'bridge' AA' forms. Along the ring AA' the radius of curvature in the plane of the figure is very small. As a consequence of surface tension, the pressure in the liquid is therefore very small also.

can be established. This is essentially the sequence of events proposed by Chapman & Critchlow (1967) in their study of vortex rings formed by falling drops. Our findings show however that this picture is incorrect.

Before describing the results of the detailed calculations, we shall consider the matter in a rather heuristic fashion in the next section. There we show that even for moderate impact velocities contact between the opposing liquid surfaces is established at a number of points. Since just before coming into contact each point carries its own value of the velocity potential, a vortex sheet is formed, which eventually rolls up into the well-known ring vortex that appears in these conditions (Rogers 1858; Thomson & Newall 1885; Batchelor 1967; Chapman & Critchlow 1967; Carroll & Mesler 1981; Rodriguez & Mesler 1988; Esmailizadeh & Mesler 1986). It appears therefore that this vortex ring is not due to viscous effects, as might be thought.

The present work was motivated by an attempt to study the mechanism by which a bubble is produced at the bottom of the crater formed by a drop hitting a water surface (Franz 1959; Pumphrey & Crum 1988; Pumphrey, Crum & Bjorno 1989). The oscillation of this bubble seems to play a very important role in the noise produced by rain and sprays on the ocean surface (Pumphrey & Crum 1989; Pumphrey *et al.* 1989; Prosperetti, Pumphrey & Crum 1989). Our preliminary results show that the bubble is formed by a very delicate balance between surface tension and gravity. The earlier accounts of the collision process available in the literature, in which surface tension is either not considered (Harlow & Shannon 1967*a*, *b*), or included with insufficient accuracy (Nystuen 1986; Nystuen & Farmer 1988), fail therefore to simulate the collision with the necessary detail. In an effort to improve on these studies, we were led to the present investigation.

A rather unexpected result of this study is the prediction that a number of tiny toroidal bubbles should remain entrapped between the two contacting surfaces. It appears probable that these structures are unstable and quickly break up into spherical bubbles. This prediction appears to be in agreement with the observations of Blanchard & Woodcock (1957), who were interested in the formation of condensation nuclei for rain drops, and of Carroll & Mesler (1981) and Esmailizadeh

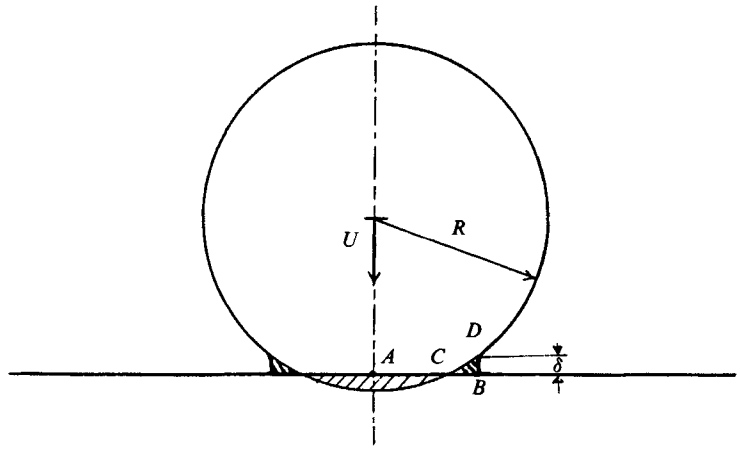

FIGURE 2. Schematic illustration of the liquid relocation process described in the text. The shaded portion of the drop indicates the volume that must be displaced outward and relocated around the ring of contact in the annular region *BCD*.

& Mesler (1986), who studied this phenomenon for its bearing on boiling heat transfer. We discuss these observations in relation to our findings in the final section.

2. Surface destruction

The basic question we wish to address is, does the line of contact between the liquid surfaces move outward fast enough to prevent further contact after the initial one, or is free surface destroyed by the surfaces coming together faster than the line of contact can move? A qualitative answer can be formulated by studying a simplified physical model. Consider for example the case of a droplet hitting a plane surface (figure 2). In the very early stages of the contact, deformation must be localized in the neighbourhood of the contacting point, and must be much greater for the drop than for the plane surface owing to the smaller inertia. We wish to show with a simple order-of-magnitude argument that, unless the impact velocity is very small, contact between the two surfaces cannot be limited to the initial point. To prove this statement we first estimate the radially outward velocity that would be necessary, on the basis of mass conservation, to prevent this further contact. Then we show from the momentum equation that this velocity is incompatible with the available pressure gradient in the early stages of the motion.

With reference to figure 2, assume that the shaded portion of the drop would relocate in the region, the trace of which on the meridian plane is *BCD*. This would be, in fact, the 'embryo' of the splash. The shape of this region evidently cannot be the one depicted, but the difference with the actual shape can only introduce constants of order one in the final results. If we set

$$\epsilon = \frac{Ut}{R}, \tag{1}$$

where U is the impact velocity, R the drop radius, and the time t is measured from the instant of first contact, elementary geometrical considerations lead to the

following equation relating the length δ of the segment BD to ϵ:

$$\left(\frac{\delta}{R}\right)^3+\left(\frac{\delta}{R}\right)^2\epsilon=\epsilon^3. \tag{2}$$

In obtaining this relation we have assumed $\delta/R = O(\epsilon)$, which will be confirmed *a posteriori*, and we have dropped higher-order terms. The solution of the above equation gives

$$\frac{\delta}{R}=a\epsilon, \tag{3}$$

where a is a numerical constant approximately equal to 0.903 for the assumed shape and presumably some other value close to one for more realistic shapes. If the rate of change of the volume of the 'splash' BCD is now set equal to the rate at which the shaded portion of the drop volume in figure 2 increases, as is necessary for mass conservation, it is easy to show that the radially outward velocity of the point B of figure 2 must be

$$u_B=\frac{1}{a(1+\frac{1}{2}a)}\left(\frac{RU}{2t}\right)^{\frac{1}{2}}. \tag{4}$$

The time dependence in this relation is the same as in the early stages of blunt solid-body penetration into an incompressible fluid (Korobkin & Pukhnachov 1988). If this velocity u_B is too large to be produced by the available pressure gradient, the relocation of the drop's mass into the splash cannot take place and the surfaces must move towards each other and eventually come into contact. To estimate the maximum velocity compatible with the equation of motion we proceed as follows.

For an extremely short time after the impact, the liquid pressure on the axis of symmetry at the point A in figure 2 must exceed p_0, the undisturbed ambient pressure, by an amount of the order of ρUc, where ρ is the liquid density and c is the speed of sound in the liquid. This large pressure must fall to a level of the order of the stagnation pressure in a time comparable with the acoustic travel time between A and neighbouring surface points such as B. This timescale is much shorter than those we consider and can therefore be neglected for the present purposes so that we may take $p_A \approx p_0+\frac{1}{2}\rho U^2$. The pressure at B, just inside the liquid, must be $p_0-\sigma\mathscr{C}$, where σ is the surface tension coefficient and $\mathscr{C}$, the local curvature, may be estimated to be

$$\mathscr{C}\approx\frac{1}{aUt}\left[1-\frac{a}{2+a}\left(\frac{2Ut}{R}\right)^{\frac{1}{2}}\right]. \tag{5}$$

Here the inverse of the first term is an estimate of the radius of curvature in the plane of the drawing of figure 2, while the second term is the inverse of the length AB, which is the radius of curvature in the orthogonal direction. From the equation of motion we then obtain

$$\frac{\mathrm{d}u_B}{\mathrm{d}t}=-\frac{1}{\rho}\frac{\partial p}{\partial r}\approx-\frac{p_B-p_A}{\rho r_B},$$

where u_B has the same meaning as before and r_B is the length AB. By use of the previous estimates for p_A and p_B this gives

$$\frac{\mathrm{d}u_B}{\mathrm{d}t}\approx-\left(\frac{R}{2Ut}\right)^{\frac{1}{2}}\left\{\frac{\sigma}{a\rho RUt}\left[1-\frac{a}{2+a}\left(\frac{2ut}{R}\right)^{\frac{1}{2}}\right]+\frac{U^2}{R}\right\}. \tag{6}$$

This represents an estimate of the outward acceleration of the line of contact (point

B in figure 2) compatible with the equation of motion. The condition for the mass relocation required by continuity to be dynamically possible is that the time derivative of the estimate of u_B given in (4) be in magnitude less than or equal to this value, from which

$$\frac{1}{2+a} \leqslant \frac{\sigma}{\rho R U^2}\left[1-\frac{a}{2+a}\left(\frac{2Ut}{R}\right)^{\frac{1}{2}}\right]+\frac{atU}{R}. \tag{7}$$

At time $t = 0$, this relation requires that a quantity, which we may identify with the inverse of a Weber number We,

$$We^{-1} = \frac{\sigma}{\rho U^2 R}, \tag{8}$$

be greater than a numerical constant of order 1. With increasing time the right-hand side of (7) goes through a minimum which, for a of order 1 and We of order 1 or smaller, is still of order We, after which it grows monotonically so that the inequality (7) will be satisfied for long times irrespective of the value of We. Physically this occurs because, as the radius AB of the contact region increases (see figure 2), more and more mass can be relocated around the periphery of this region. The last term in (7), which dominates for long times, arises from the stagnation pressure term. Although our considerations are only justified for small values of Ut/R, the qualitative indication is that surface-tension effects grow increasingly small. This suggests that the stagnation pressure should eventually be able to generate enough of a pressure gradient to prevent surface contact.

The above considerations strongly suggest that destruction of free surface does occur when the impact velocity is sufficiently large, at least in the early stages of the impact process. For a water drop of 1 mm radius, $We = 1$ for $U \approx 0.25$ m/s, which is the terminal velocity of fall from a height of about 4 mm. We therefore conclude that, in most cases of practical interest, the impact of droplets on a liquid surface is accompanied by some amount of surface destruction. This consideration leads us to the next step in our analysis, namely how this destruction is effectively carried out in a manner compatible with the action of surface tension. To address this point we consider an idealized situation described in the next section.

3. Formulation of the problem

We wish to study in detail the dynamics of the flow taking place in the region where the two liquid masses come together. As was noted before, the destruction of free surface occurs in the early stages of the impact and is therefore limited to the vicinity of the point of initial contact. This circumstance suggests that the essential features that we wish to study will be preserved if, in order to reduce the number of parameters, we simplify the geometry of the problem as shown in figure 3. Two semi-infinite masses of inviscid, incompressible liquid are connected by a 'bridge'. This configuration has an axis of symmetry SS' which goes through the centre of the 'bridge' and which is taken as the z-axis. In addition, it possesses a plane of symmetry TT', as indicated in the figure, which is taken as the (x, y)-plane. The liquid at infinity is in a state of rigid-body motion with velocity $\mp U$ along the z-axis, constant with time. Initially the bridge is bounded by the surface of a half-torus the cross-section of which will be chosen in a number of ways in the numerical results to be described. The half-torus joins with a zero tangent two parallel planes separated by a distance δ. The radial coordinate of the point of the toroidal surface closest to

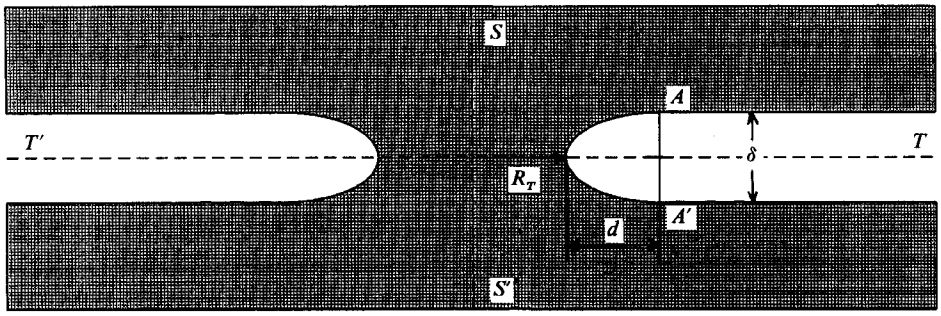

FIGURE 3. Simplified geometry for the study of the surface destruction problem. Two semi-infinite masses of liquid that approach each other with a velocity U are connected by a 'bridge'. The axis of symmetry is denoted by SS' and the plane of symmetry by TT'.

the axis of symmetry will be denoted by $R_T(t)$, and the radial coordinate of the points where the torus joins the planes in the initial configuration by $R_T(0)+d$. It is desired to study the evolution of this system when released.

Of course, the long-time aspects of the process will be influenced by the curvature of the contacting surfaces that we disregard here. The qualitative consequences of this curvature are readily understood and will be pointed out below. In any case, their consideration is more appropriate for studies devoted to specific problems (e.g. the impact of a rain drop on a liquid surface, which will form the object of a separate publication) rather than in an analysis, such as the present one, devoted to the basic and hopefully universal features of the process of present concern. A further approximation that we introduce is the neglect of viscous effects. While we shall return on this point at the end of §4 to show that this procedure is justified for low-viscosity liquids, it may be noted here that the predictions of an inviscid model are of interest in themselves in view of the frequent use of such a model in the study of free-surface flows. Finally, since the physical scales for the applications that we have in mind are very small, we are justified in neglecting the effect of gravity.

It is somewhat disappointing that, even with the great reduction in the complexity of the problem afforded by the foregoing approximations, it has proven impossible to make progress by purely analytical means. It appears that this problem differs in an essential way from other, superficially similar ones that can to some degree be studied analytically. Taylor (1959) and Taylor & Michael (1973) studied the growth of holes in liquid sheets, and Keller & Miksis (1983) considered idealized models of breaking liquid threads and films. In the present case the existence of intrinsic lengthscales such as δ, R_T and d prevents the existence of similarity solutions such as those found by Keller & Miksis. The growth of a 'bridge' rather than a hole has the consequence that mass conservation cannot be exploited as was done by Taylor. We are thus forced to use a numerical approach that we base on a variant of the boundary-integral method (Jaswon & Symm 1977; Baker, Meiron & Orszag 1982, 1984).

With the hypotheses and approximations described above, it is possible to describe the velocity field in terms of a velocity potential which is taken to have the form $\phi_* - U_*|z_*|$, where

$$U_* = \frac{U}{(\sigma/\rho\delta)^{\frac{1}{2}}}, \tag{9}$$

is the dimensionless approach velocity and $z_* = z/\delta$. From now on we shall use exclusively quantities made dimensionless with respect to the initial separation of the planes δ and the characteristic time $(\rho\delta^3/\sigma)^{\frac{1}{2}}$, but we shall omit the asterisks. It may be noted that, in these units, the dimensionless time t_{close} necessary for the two planes to touch is

$$t_{\text{close}} = \tfrac{1}{2}We^{-\frac{1}{2}}, \tag{10}$$

where the Weber number is now based on δ rather than on R as in (8).

From the Laplace equation satisfied by the velocity potential we derive the following equation for ϕ:

$$\nabla^2\phi = 2U\delta(z), \tag{11}$$

where $\delta(z)$ is the delta distribution. By use of the Bernouilli integral to calculate the pressure and of the dynamic boundary condition that the pressure difference be balanced by the Laplace pressure, it is easy to obtain the following evolution equation for the value of ϕ on the free surface:

$$\frac{\mathrm{d}\phi}{\mathrm{d}t} = \tfrac{1}{2}|\nabla\phi|^2 - \tfrac{1}{2}U^2 + \mathscr{C}. \tag{12}$$

Here the convective derivative on the left-hand side is with the total velocity $\mp U + \nabla\phi$ and initially $\phi = 0$.

Integration of (12) in time gives the value of ϕ on the free surface and allows one to calculate the velocity in the direction tangent to this surface. To calculate the velocity in the normal direction we make use of Green's formula to find, after integration over the angular variable,

$$\phi = -2U\int_0^{r(0)} G\Big|_{z=0}\,\mathrm{d}r + \int_S \left(G\frac{\partial\phi}{\partial n} - H\phi\right)\mathrm{d}s. \tag{13}$$

This relation is treated as an integral equation for the derivative $\partial\phi/\partial n$ of ϕ in the direction normal to the free surface and oriented away from the liquid. The first term arises from the delta-function inhomogeneity in (11) and corresponds to the volume integral in Green's formula. The surface integral that appears in Green's formula has been reduced by the angular integration to an integral over the trace S that the free surface leaves on a (half) meridian plane. The functions G and H are defined by Jaswon & Symm (1977) as

$$G = \frac{2r}{\pi}\frac{K}{A^{\frac{1}{2}}}, \quad H = \frac{2r}{\pi}\frac{\partial}{\partial n}\frac{K}{A^{\frac{1}{2}}}, \tag{14}$$

where

$$A = (R+r)^2 + (Z-z)^2, \quad m = \frac{4rR}{A}, \tag{15}$$

and $K(m)$ is the complete elliptic integral of the first kind and modulus m. In (14) and (15) R and Z denote the cylindrical coordinates of the surface point at which ϕ is evaluated on the left-hand side of (13), while r, z are the coordinates of the integration point. It may be remarked that, although the Fredholm integral equation (13) is of the first kind, the fact that the kernel G exhibits a logarithmic singularity substantially mitigates the numerical problems usually associated with the ill-posedness of such equations.

To solve numerically (13) for $\partial\phi/\partial n$ we use cubic splines to interpolate ϕ, r and z,

and piecewise linear functions to interpolate $\partial\phi/\partial n$. Beyond some large distance from the axis of symmetry the following approximations for ϕ and $\partial\phi/\partial n$ are used to perform the integrations:

$$\phi = \phi_{\mathrm{F}}\frac{r_{\mathrm{F}}}{r}, \quad \frac{\partial\phi}{\partial n} = \left(\frac{\partial\phi}{\partial n}\right)_{\mathrm{F}}\frac{r_{\mathrm{F}}^2}{r^2},$$

where the subscript F denotes the last node on the surface. Details concerning the use of splines and the formulation in general are given in Oguz (1989). Here we only mention the fact that, as is well known, in numerical calculations in which surface tension is included but not viscosity, the free surface tends to be irregular owing to the numerical excitation of short, very high-frequency, capillary waves which also have the unpleasant side effect of rendering the time integration stiff. We have applied a smoothing procedure consisting in the averaging of the surface curvature over a short interval around each node of the spline interpolation. Further smoothing was provided by redefining the spline nodes at each time step so as to keep them equispaced. An implicit, second-order accurate, predictor–corrector method with under-relaxation by a factor 0.5 was used for the time integration. Even with these precautions, the numerical results showed some surface oscillations, the presence of which cannot be real in view of the short lengthscales (of the order of microns) of present concern. For this reason we have tried adding a term simulating the effect of viscous stress to (12). Several cases with and without this term have been tried and its effect was found to be confined to the attenuation (although not a complete removal) of the high-frequency capillary waves, as desired. Our extensive experience with the program, which has been satisfactorily applied to several situations in some of which comparison with analytical solutions was possible, and a series of convergence tests (see below at the end of §4), leads us to believe that the results to be shown are essentially accurate.

4. Zero velocity

To study the problem stated in the previous section it proves useful to consider first the case of zero approach velocity. Figure 4 presents several snapshots of the free surface at different times for this case. In view of the axial symmetry only the trace on a meridian half-plane is shown. The complete three-dimensional picture is obtained by rotating the figure around its left margin, which coincides with the axis of symmetry.

After the non-dimensionalization described in §3, for zero velocity of approach, the only quantities characterizing the calculation are the shape of the cross-section of the torus and the value of $R_T(0)$. This figure corresponds to $R_T(0) = 1$. The cross section has been taken to be elliptical, with a 2:1 ratio of the axes, so that the distance d defined in figure 3 is 1. The initial shape of the surface evolves into two symmetric capillary waves which, in the three-dimensional picture, indent the liquid masses with two circular channels of progressively increasing radius. These two channels are joined and bounded towards the axis of symmetry by a nearly 'flat' front which seems to be the distinctive feature of the problem. We have found the same behaviour in all the cases that we have calculated, irrespective of the shape of the cross-section of the initial torus. For example, we show in figure 5 a similar sequence of surface shapes (taken at the same times as those shown in figure 4) for a case in which $R_T(0) = 1$ as before, but the initial cross-section is circular so that $d = \frac{1}{2}$.

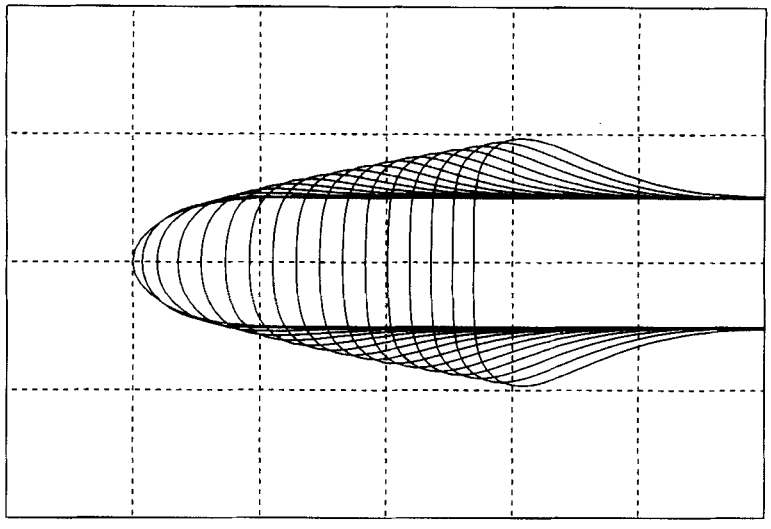

FIGURE 4. Successive computed positions of the free surface for the liquid 'bridge' problem of figure 3 and zero velocity. The dimensionless time between traces is 0.16 and corresponds to 8 time steps. Only the traces of the surface on a half-meridian plane are shown. The complete configuration is obtained by rotating the figure around its left margin, which is the axis of symmetry. The initial shape of the cavity 'nose', which is the leftmost trace, is a half-ellipse of aspect ratio 2. The motion is away from the axis of symmetry towards the right. Here and in the following figures the dimensionless spacing of the dotted grid is unity.

Except for the first few shapes, the result is very nearly identical to the previous case and the surface contours are nearly superposable.

In figure 6 the velocity

$$V_* = \frac{V}{(\sigma/\rho\delta)^{\frac{1}{2}}} \quad \text{(positive outward)} \tag{16}$$

of the point located at the intersection with the plane of symmetry is shown for the previous two cases. Surface oscillations are very evident, even though the shapes shown in figures 4 and 5 look smooth. The velocity V_* very quickly rises to a value close to 1 and then slowly decays with time. The only noticeable difference between the two cases is during the initial phase. For a gap width $\delta = 1$ μm, $V_* = 1$ is equivalent, for water, to $V \approx 8.5$ m/s. Furthermore, with the present non-dimensionalization, $V_* = 1$ corresponds to the phase speed of a capillary wave with wavenumber $1/\delta$.

It is interesting to compare this result with the rough estimate, (4), obtained in §2 for the speed necessary to relocate mass without further surface contact. If, as seems reasonable, we take the present gap width δ to coincide with the length δ defined in figure 2, and we use (3) for this quantity, we find, from (4),

$$u_{B*} \approx 0.57 We^{\frac{1}{2}},$$

where the numerical constant has been evaluated using the value of a given in §2. A drop with a radius of $R = 1$ mm has a terminal velocity $U \approx 6.6$ m/s (Dingle & Lee 1972) which results in $u_{B*} \approx 13.9$, which is seen to be one order of magnitude larger than the velocity V_* given by the numerical solution.

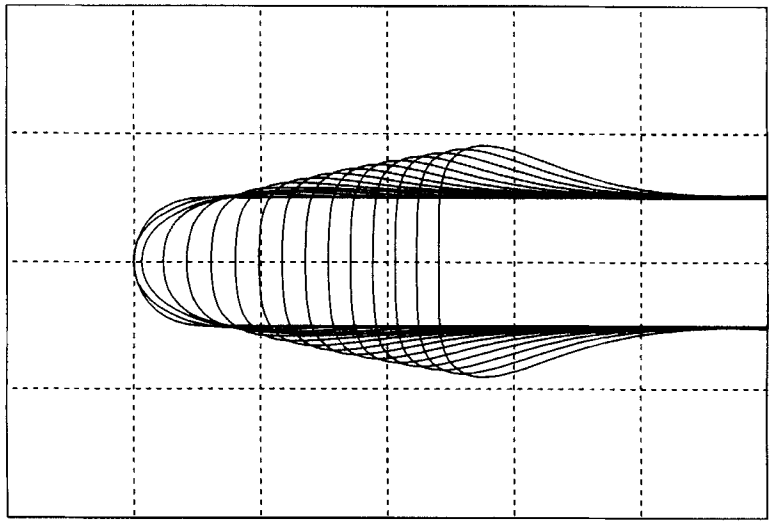

FIGURE 5. Successive computed positions of the free surface for the liquid 'bridge' problem of figure 3 and zero velocity. Here the initial shape of the cavity 'nose', which is the leftmost trace, is a half-circle of unit radius. The dimensionless time between traces is 0.16 and corresponds to 8 time steps. Only the traces of the surface on a half-meridian plane are shown. The complete configuration is obtained by rotating the figure around its left margin, which is the axis of symmetry. The motion is away from the axis of symmetry towards the right.

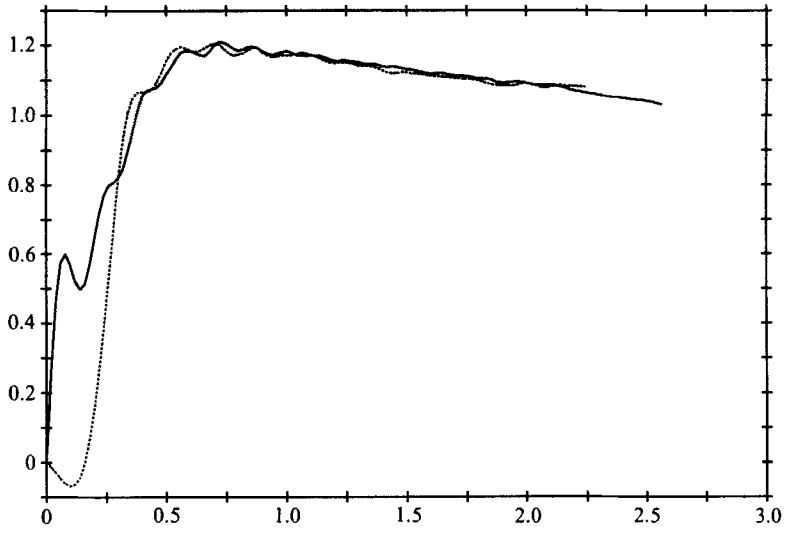

FIGURE 6. Dimensionless velocity V_* of the free surface at the plane of symmetry (i.e. the point closest to the z-axis) versus dimensionless time. The continuous line is for the elliptic initial shape of figure 4 and the dotted line for the circular one of figure 5.

The amplitude of the capillary wave, defined as the maximum value of $|z|$ for a given surface shape, is also clearly growing in time. We show in figure 7 a graph of this quantity as a function of time for the two cases considered before. Again oscillations are apparent although the two results are extremely close. As already stated, we found essentially the same behaviour in all the cases that we have

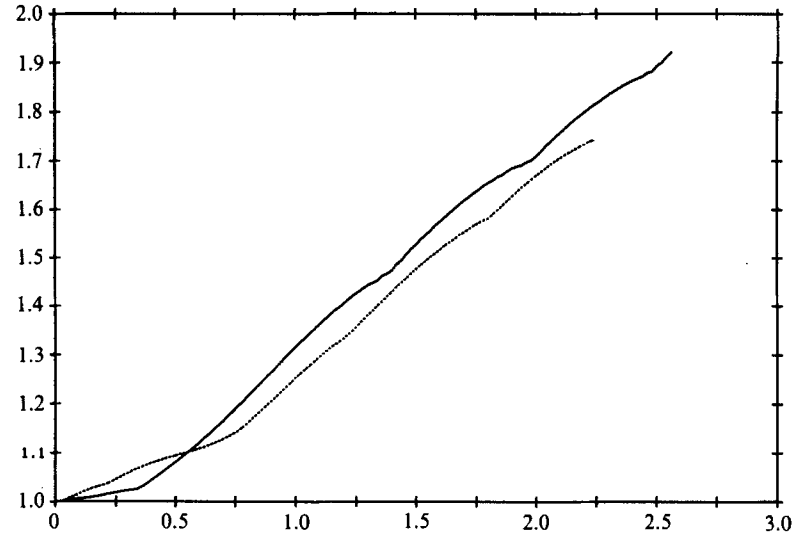

FIGURE 7. Amplitude of the capillary wave, defined as the maximum value of $|z|$ for a given surface shape, versus time for the two cases of figure 4 (continuous line) and 5 (dashed line).

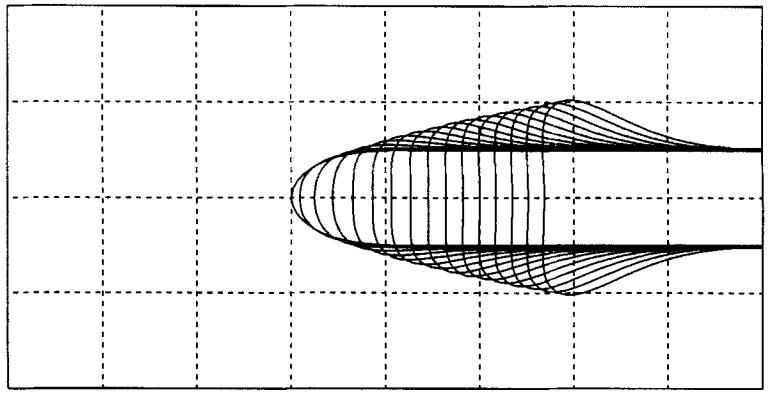

FIGURE 8. Successive positions of the free surface for the liquid 'bridge' problem for a larger initial distance from the axis of symmetry (left-hand margin of the figure), $R_T(0) = 3$, and the same initial shape as in figure 4. The motion is away from the axis of symmetry towards the right. The dimensionless time interval between successive traces 0.16 and corresponds to 8 time steps.

investigated, and we are therefore confident that the evolution of the process is rather insensitive to the initial conditions.

Another important parameter in this problem is the value of $R_T(0)$. We show in figure 8 the results for $R_T(0) = 3$ and $d = 1$, with a 2:1 elliptical initial shape, again at the same times as in figures 4 and 5. The 'flat' advancing front proves to be the basic feature of the result in this case as well. The velocity graph in figure 9 has a behaviour qualitatively very similar to that shown in figure 6, but the peak velocity is now somewhat larger. Presumably this is due to the combined effect of a reduction of the competing curvature in the orthogonal plane, and to the release of more surface energy due to the geometry. The dotted line in figure 9 is the result obtained by computing the curvature by fitting circular arcs to the surface points rather than from the spline interpolation. The minor differences between the two results confirm

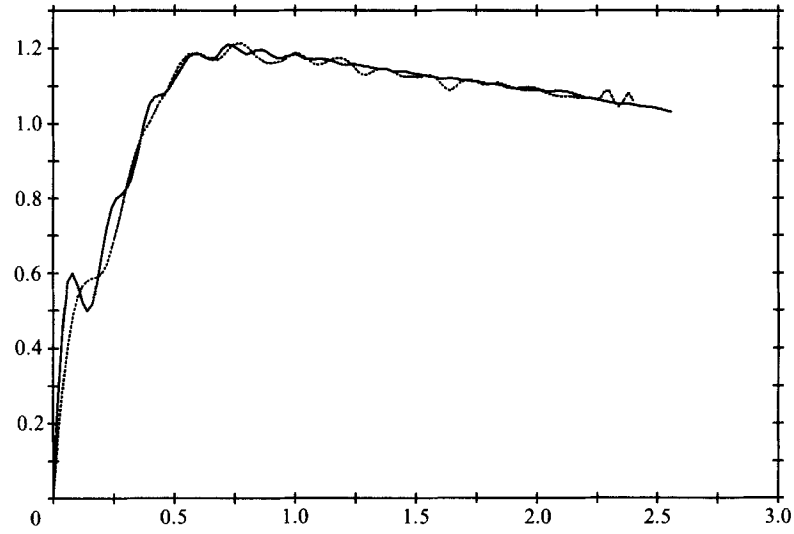

FIGURE 9. Dimensionless velocity V_* of the free surface at the plane of symmetry (i.e the point closest to the z-axis) versus dimensionless time for the case of figure 8. Cubic splines were used to calculate the surface curvature for the result shown by the continuous line. For the dotted line use was made of circular arcs fitted to the computed points.

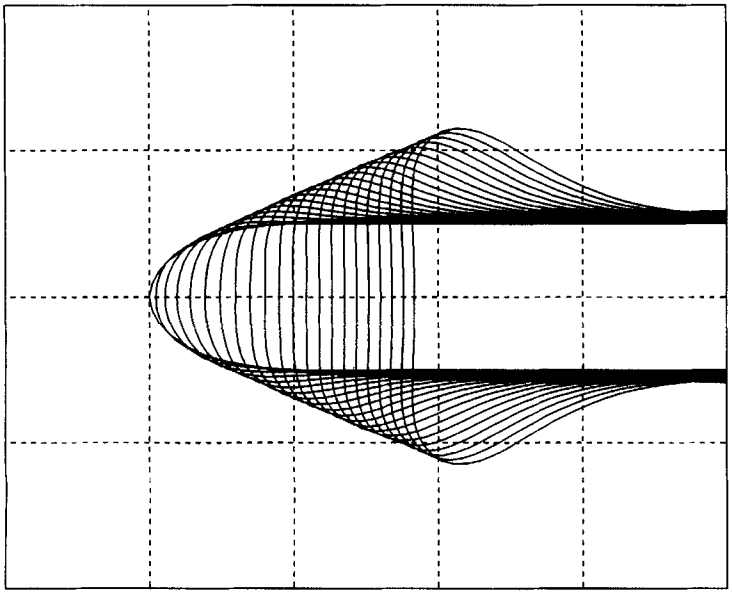

FIGURE 10. Successive positions of the free surface shapes for the two-dimensional case. The initial shape is the same as in figure 4 (half-ellipse of aspect ratio 2). The fluid extends to infinity in every direction except the gap in the right and there is no symmetry with respect to the left margin in this geometry. The motion is towards the right. The dimensionless time interval between successive traces is 0.08 and corresponds to 4 time steps.

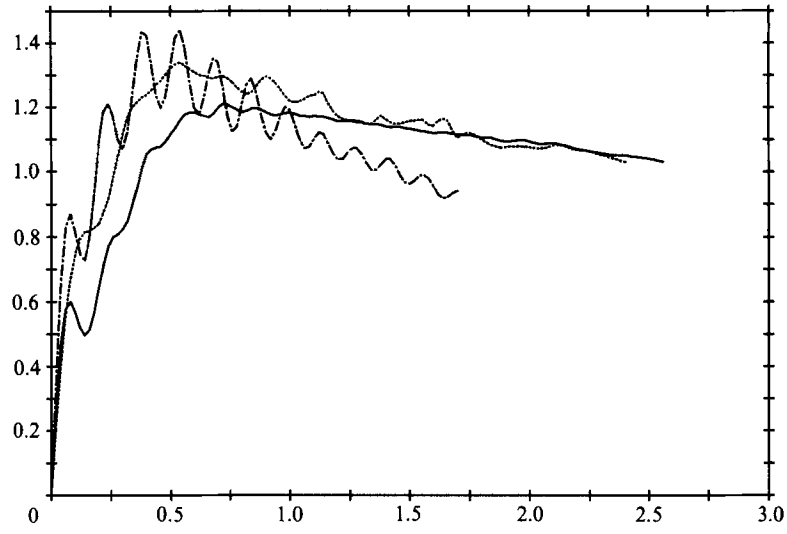

FIGURE 11. Comparison of the velocity of the points on the plane of symmetry for the cases in figure 4 (——); figure 9 (...); and figure 11 (—.—.).

that the slight irregularities of the curves arise from capillary waves. At the same time, the substantial agreement of the two computations suggests that the basic features of our results are unaffected by the way in which the effects of capillarity are stabilized.

As $R_T(0)$ increases further the effect of the curvature in the planes orthogonal to those of the figures decreases and the situation becomes closer and closer to being two-dimensional rather than axisymmetric. For completeness we present in figure 10 the results for an exactly two-dimensional situation for an initial shape identical to that of figure 4. The snapshots of the surface are shown at the same times as in that figure. In this case the left margin of the figure is placed arbitrarily and is not a plane of symmetry. These results have been obtained by using an integral equation of the same form as (13) but with the functions G and H given by

$$G = -\frac{1}{2\pi}\log \boldsymbol{h}\cdot\boldsymbol{h}, \quad H = \frac{1}{\pi}\frac{\boldsymbol{n}\cdot\boldsymbol{h}}{\boldsymbol{h}\cdot\boldsymbol{h}}. \tag{17}$$

Here $\boldsymbol{h}$ is the vector with components $X-x, Z-z$ where X, Z and x, z are the coordinates of the observation and integration points respectively. The computation is otherwise the same as before. In this case we found the results to be more sensitive to the treatment of the condition at 'infinity'. Since no useful asymptotic form similar to the one previously used is available for this geometry, it was necessary to simply truncate the integration by setting $\phi = 0$, $\partial\phi/\partial n = 0$ at some large distance from the axis of symmetry. The minor opening of the horizontal lines with time is caused by the error introduced by this procedure. Indeed, it was found that this opening decreased by enlarging the computational domain. Since we show these results for comparison purposes only, it did not seem worthwhile to invest a greater effort in an attempt to solve this minor problem. The velocity of the points on the plane of symmetry for this case is compared in figure 11 (dash-and-dot line) with those of figures 4 (continuous line) and 9 (dotted line). The two-dimensional calculation appears wavier than the others because it was run with a coarser resolution in view of the need for a larger computational domain. The trends are

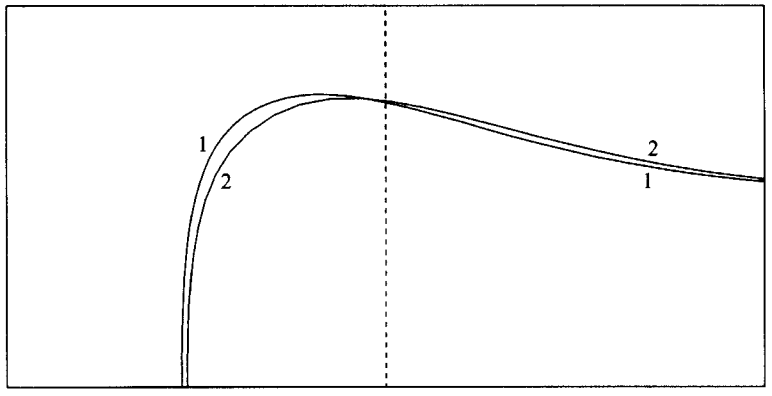

FIGURE 12. Comparison of the free-surface shapes at the dimensionless time 1.440 for the case of figure 4 computed with two different spatial resolutions, $\Delta s = 0.1$, line 1, and $\Delta s = 0.2$, line 2. The two squares are the third and fourth of the second row from the top in figure 4.

however similar. A very rapid initial rise brings the velocity to a value somewhat above that found for $R_T(0) = 3$, thus confirming the trend towards higher maximum velocities as $R_T(0)$ increases. The decline from this value is however faster than in the other cases, which also agrees with the difference found between $R_T(0)$ equal to 1 and 3.

At the other extreme, if $R_T(0)$ is very small, the curvature in the plane of symmetry of the system, which has a sign opposite to that in the meridian plane, dominates. The free surface, rather than moving outward, moves inward toward the axis of symmetry until the 'bridge' pinches off and the two liquid masses are eventually severed from each other. The critical value of $R_T(0)$ below which this happens is somewhat dependent on the initial shape but is close to the radius of curvature of the initial shape at $z = 0$ in the meridian plane. With this value of $R_T(0)$ the initial curvature at $z = 0$ vanishes.

One may speculate to what extent these results would be affected by viscosity. It is well known that, for a surface wave of wavenumber k, viscous effects act on timescales of the order of $(\nu k^2)^{-1}$ where ν is the kinematic viscosity coefficient. If we use the estimate $k \sim \delta^{-1}$, the viscosity of water, and δ of the order of microns, we find that this timescale is much longer than the timescale $(\rho\delta^3/\sigma)^{\frac{1}{2}}$ that is relevant for the present problem. It seems reasonable therefore to conclude that the main features of our findings would not be affected by viscosity. This conclusion seems also to be in agreement with experiment, as will be mentioned below.

As a final point of interest we present an example of the convergence of the numerical method in figure 12 where we show a detail of the shape of the interface at time 1.440 as computed with two different resolutions ($\Delta s = 0.1$, line 1, and $\Delta s = 0.2$, line 2) for the case of figure 4. The agreement between the two simulations is very good, especially in consideration of the very delicate stability features of the present problem.

5. Non-zero velocity

The effects due to a non-zero velocity of approach of the two liquid masses can be inferred to some extent from the previous results, but unexpected features do arise. In figure 13 we show the case of figure 4 with a velocity $U_* = 0.2$ superposed. The

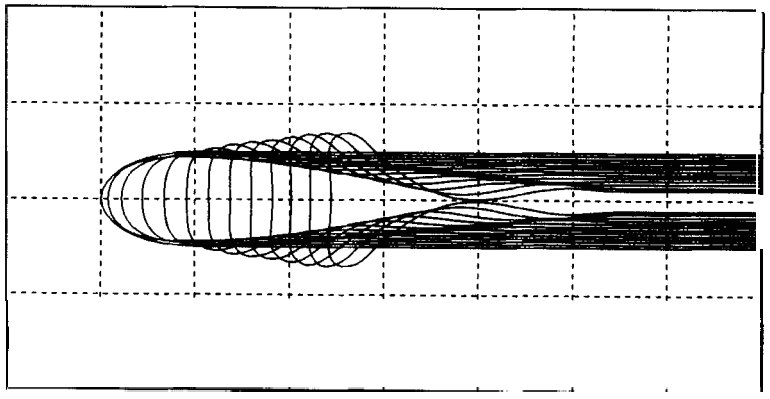

FIGURE 13. Successive computed positions of the free surface for the axisymmetric liquid 'bridge' problem of figure 4 and a dimensionless approach velocity of the liquid masses of 0.2. The initial shape is the same as in figure 4. The left margin is the axis of symmetry. The motion is towards the right. The dimensionless time interval between successive traces is 0.16 and corresponds to 8 time steps.

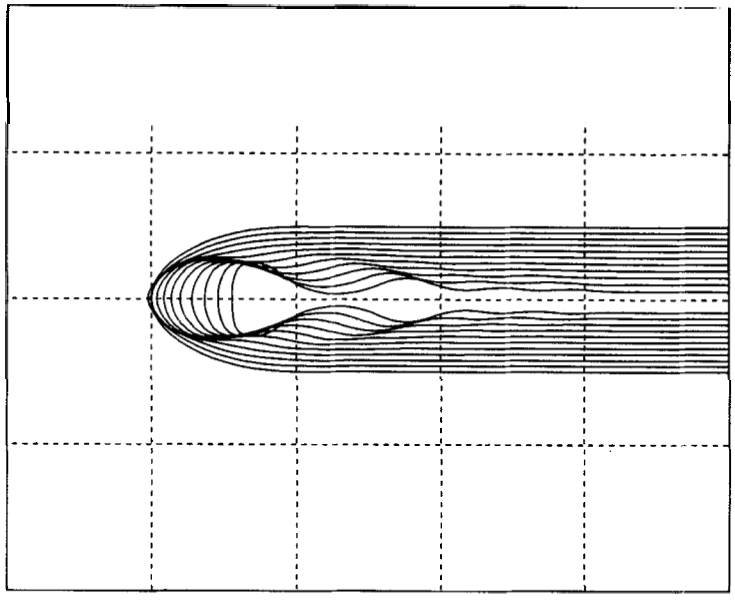

FIGURE 14. Successive computed positions of the free surface for the axisymmetric liquid 'bridge' problem of figure 4 and a dimensionless approach velocity of the liquid masses of 1. The initial shape is the same as in figure 4. The left margin is the axis of symmetry. The motion is towards the right. The dimensionless time interval between successive traces is 0.04 and corresponds to 4 time steps.

characteristic troughs of the capillary waves of the zero-velocity case are still present, but they are accompanied downstream by two wave crests which are found to be dependent on the initial shape. This feature can be appreciated by comparing figures 14 and 15, which correspond to $U_* = 1$. For figure 14 the initial shape is the same 2:1 ellipse of figure 4, 8, and 10 with $R_T(0) = 1$ and $d = 1$. For figure 15 it is a circle as in figure 5. The velocity of the points on the plane of symmetry is compared in figure 16 (dash-and-dot line) with that of the zero-velocity case of figure 4

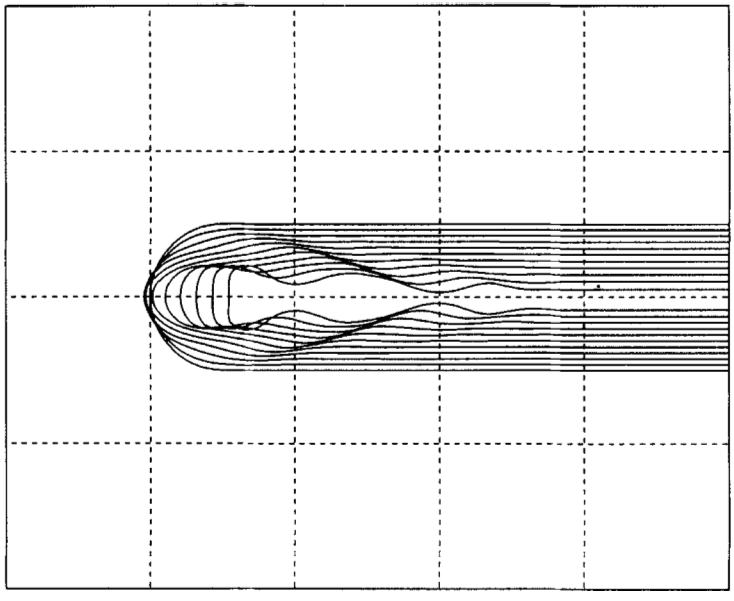

FIGURE 15. Successive computed positions of the free surface for the axisymmetric liquid 'bridge' problem of figure 4 and a dimensionless approach velocity of the liquid masses of 1. The initial shape is semi-circular as in figure 5. The left margin is the axis of symmetry. The motion is toward the right. The dimensionless time interval between successive traces is 0.04 and corresponds to 4 time steps.

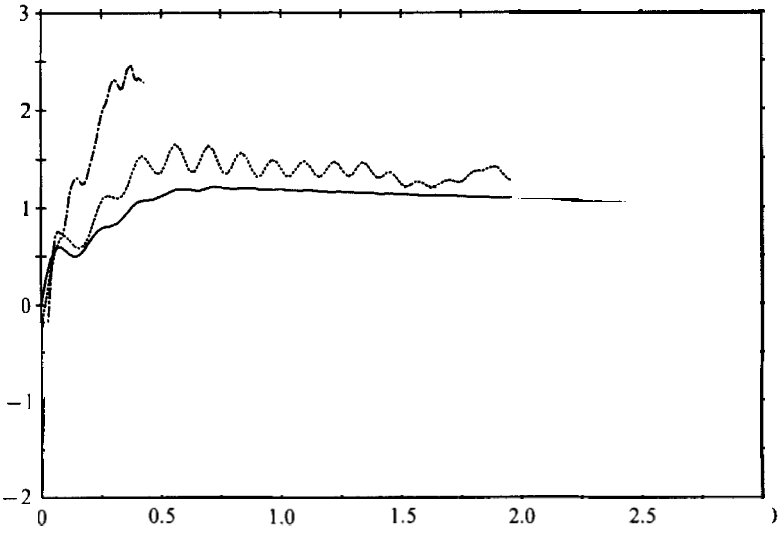

FIGURE 16. The velocity of the points on the plane of symmetry for different approach velocities: ——, $U_* = 0$; ..., 0.2; —·—·, 1.0. The initial shape is elliptical as in figure 4.

(continuous line) and that for $U_* = 0.2$ of figure 13 (dotted line). Clearly a non-zero approach velocity leads to a faster outward velocity, but there is no indication of this latter velocity becoming greater and greater as the gap narrows, as might have been expected on intuitive grounds. Furthermore, it is evident that the appearance of the

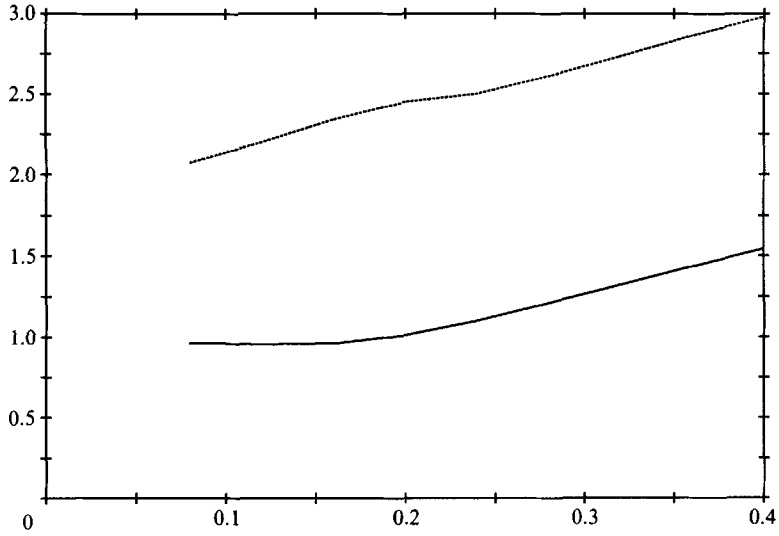

FIGURE 17. The motion of the rightmost wavecrest for the case of figure 15 (upper line) compared with that of the point on the plane of symmetry (lower line).

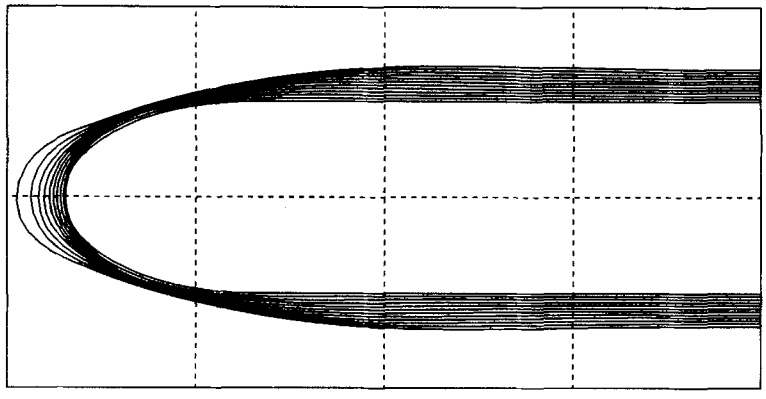

FIGURE 18. Successive computed free-surface shapes of a liquid 'bridge' being pulled apart with a dimensionless velocity of 0.2. The initial distance closest to the axis of symmetry (left margin) is $R_T(0) = 0.3$ and the initial shape is a half-ellipse of aspect ratio 2 as in figure 4. In this case the motion is towards the left and the last computed shape is the one closest to the axis of symmetry. With zero velocity this case exhibits a motion towards the right as in all other cases shown. The dimensionless time interval between successive traces is 0.16 and corresponds to 8 time steps.

two symmetrically placed wave crests will lead to further contact between the liquid masses. When this happens, the resulting cusp will very rapidly relax toward a shape with a continuous curvature, after which the process may be envisaged as repeating itself indefinitely on a smaller and smaller scale. We shall discuss the significance of these conclusions in the last section.

It is also of some interest to compare the motion of the rightmost wave crest with that of the point on the plane of symmetry. We show in figure 17 the positions of these two points (upper and lower lines, respectively) for the case of figure 15. After an initial interval, the two traces are close to being parallel, which indicates that the evolution of the wave structure is characterized by wavenumbers of similar magnitude in its various parts.

Although irrelevant for the drop impact problem, for completeness we also give one example of the effect of a negative velocity U_*, which would correspond to the two liquid masses being pulled apart. This is shown for a velocity $U_* = -0.2$ in figure 18. Here $R_t(0) = 0.3$ and $d = 1$. With a zero velocity this initial configuration is found to evolve similarly to the other examples shown with the liquid bridge becoming thicker and the free surface moving to the left. The pulling apart of the liquid masses however causes the reverse to happen and the bridge to eventually break up.

6. Discussion

If, as the two liquid masses approach, the free surface were to retain essentially its shape, with only an increase in curvature at the points on the plane of symmetry, one would expect that the radial velocity of these points would increase without bound as the gap becomes narrower and narrower (figure 1). This argument was at the basis of our early belief that no surface contact would occur after the initial one. The result of this investigation is however quite the opposite. The free surface becomes nearly 'flat' in the region of the plane of symmetry, and therefore the outward velocity is only slightly affected by the narrowing of the gap. Further contact will then occur downstream of the first one, at the crests of the capillary waves that appear so prominently in figures 13–15. After this contact is established, the process starts over again from the contact point and so on.

The large-time, large-distance behaviour in the model problem studied is not very relevant for the drop impact situation, since in this case the fact that the opposing surfaces are not (both) plane will start to play a role at some point. As the distance between opposing points on the two surfaces increases owing to their curvature, a longer time will be needed to establish contact, and this time may become sufficient for the available pressure gradient to push the liquid outward and prevent further surface contact. Curvature should however be negligible in the neighbourhood of the point of first contact, and our results should apply there. The indications furnished by these results point toward repeated contacts along a finite, and probably not too large, number of rings of increasingly larger radius. A rather unexpected prediction is that these contact regions will be separated by toroidal 'air' bubbles as sketched in figure 19.

Two questions come immediately to mind, namely, are these bubbles real, and, can they be observed? On the first point, all we have proved is that their generation seems to be the inescapable conclusion to which the model of perfect fluids with surface tension leads. Insofar as this model is widely used, our result may have some interest whether it corresponds to the actual behaviour occurring in nature or is only an artifact of the model. If we can venture into some speculation, however, we may add that one feature of our result appears to be physically correct, and therefore should survive the inclusion of more realistic effects such as viscosity. We refer to the fact that the flow in the region close to the points where two liquids come into contact is predicted to be inherently unsteady. The initial cusp rounds off instantly, moves outwards for a while becoming flatter, a new contact is established downstream of the first one, and the process repeats. If this were not so, the cusp would have to persist and propagate over intervals of time comparable with those of the fluid flow. This is incompatible with the assumption of local thermodynamic equilibrium which underlies standard fluid mechanics and, in particular, the usual treatment of surface tension. A configuration with cusps is one of large non-equilibrium and must

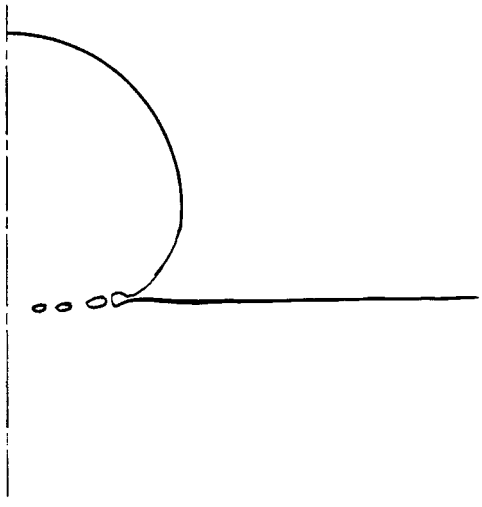

FIGURE 19. Schematic of the proposed mechanism of surface destruction by creation of a series of successive toroidal bubbles.

disappear over times very short compared with those associated with the liquid flow.

As to the second question about the observability of the toroidal bubbles it may be noted that their size is very small, comparable with the distance between the two opposing liquid surfaces in the region of contact. At the moment at which the liquid surface entraps the bubble, the pressure in it will be atmospheric, while the equilibrium pressure compatible with surface tension would be higher. For a bubble size in the range from 10 to 1 μm the overpressure due to surface tension is, in water, of the order of 0.1 to 1 atm. The toroidal bubble will therefore tend to collapse and presumably break up in the process. We base the last statement on two considerations arising in the somewhat similar case of cylindrical bubbles. In the first place a cylindrical cavity, much as a cylindrical jet, is unstable in the presence of surface tension (Chandrasekhar 1961). Secondly, a stability analysis of a collapsing cylindrical cavity (Birkhoff 1954) reveals an instability having the same origin as the one appearing in the more usual spherical case (Plesset 1954). It may also happen that the axial symmetry forced on our calculation is destroyed in nature. This will certainly be the case if contact at different points along the ring takes place at times separated by an interval longer than that necessary for the disappearance of the cusp, and is therefore very probable. In this case the formation of spherical bubbles does not have to rely on the breakup of a primary toroidal structure. An additional factor is that, unless the liquid is saturated with gas, the small spherical bubbles would tend to dissolve in relatively short times (Epstein & Plesset 1950). Even if real, therefore, the structures that we have found may not lend themselves to a casual observation. In spite of this, experimental evidence of their formation has been reported, to which we now turn.

The toroidal bubbles, or bubble chains, predicted by our study form exactly on the vortex sheet produced by the surface destruction process. They therefore seem likely to remain entrained in the vortex ring into which the sheet evolves. Precisely such an entrainment has been noticed by Blanchard & Woodcock (1957) and Carroll &

Mesler (1981). The first authors report that a 2.2 mm diameter drop at terminal velocity 'was observed to produce from 50 to 100 bubbles that were often carried down in a vortex ring to depths of 2–4 cm. The vast majority of these bubbles appeared to be under 50 microns diameter.... These bubbles would go rapidly into solution or grow depending upon whether the sea water was considerably under- or over-saturated, respectively'. The terminal velocity for a 2.2 mm drop is about 6.9 m/s (Dingle & Lee 1972) with a Weber number, given by (8), of 1.39×10^{-3} which should lead, according to the considerations of §2, to a substantial amount of free surface destruction. Blanchard & Woodcock go on to say that 'with increasing drop size an increase in the number of bubbles was observed, although the bubble size was predominantly the same'. This observation is also compatible with our findings since the toroidal bubbles are formed when the two surfaces come together, a local process which should be independent of the global lengthscales. Interestingly enough 'the larger drops also produce several bubbles of about a mm diameter'. These bubbles are very likely those formed by the pinching off of the crater, to which reference was made in §1.† It is evident from the experimental observations that the two types of bubbles are completely distinct.

The entrainment process discovered by Blanchard & Woodcock was later studied in more detail by Carroll & Mesler (1981) and Esmailizadeh & Mesler (1985). This investigation was motivated by the observation by Mesler (1981) and Bergman & Mesler (1981) that the vortex bubbles could act as boiling nuclei in hot liquids and considerably increase the heat transfer, particularly in the boiling of thin liquid layers. We reproduce in figure 20 one of Carroll & Mesler's photographs with a sketch illustrating the process. Carroll & Mesler also found that the bubbles were seen only for relatively low impact velocities, corresponding to release heights of 10 cm or less. This trend is not incompatible with our results since it is clear upon comparison of figures 13 and 14 that the size of the entrapped bubble should decrease with increasing impact velocity. This circumstance would cause a more violent collapse and a greater rate of dissolution.

Professor Mesler pointed out to us the possibility that the small bubbles remain entrapped because of a Rayleigh–Taylor instability of the impacting drop. According to this picture, just before impact the drop would be strongly flattened by the action of the thin air film that separates it from the underlying liquid and would be subject, at the same time, to a strong acceleration directed from the air into the drop. Thin air films are certainly a possibility and are thought to explain the curious phenomenon of drops 'floating' over liquid surfaces as in a low-temperature Leidenfrost effect. This phenomenon, however, is only seen by carefully depositing the drop on the liquid and disappears as soon as there is an impact velocity. The fastest growing wavelength in the Rayleigh–Taylor instability process is of the order of $(\sigma/\rho A)^{\frac{1}{2}}$, where A denotes the acceleration. To produce a bubble with a radius of 50 μm due to this process one therefore needs an acceleration $A \approx 28000$ m/s^2. For an impact velocity of 1–2 m/s, such an acceleration is sufficient to bring to rest a body in less than 100 μs, i.e. over a distance smaller than 100 μm, which is less than one tenth of the drop radius. Alternatively, it would seem reasonable that, if the drop

† The experiments of Pumphrey & Crum (1988) indicate that drops with a diameter greater than about 1.2 mm impacting at terminal velocity would not produce bubbles directly owing to the pinching off of the crater. Rather the drop, or drops, which fall back from the tip of the jet formed upon closure of the crater (Worthington 1908; Franz 1959) give rise to secondary craters which may pinch off to form a bubble. See also Pumphrey *et al.* (1989) and Prosperetti *et al.* (1989).

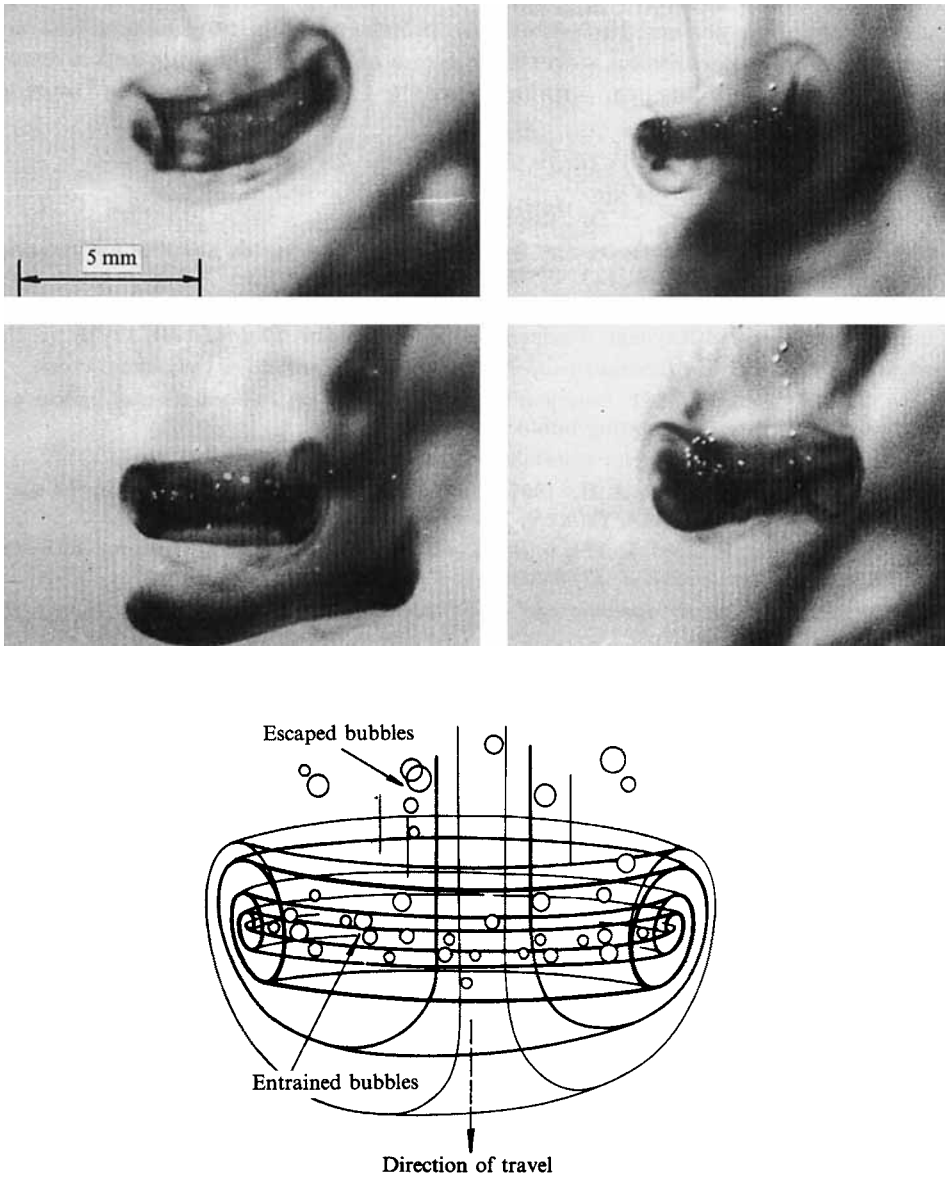

FIGURE 20. Minute bubbles entrained in the vortex ring produced by the impact of a coloured drop on a surface of the same liquid. (Courtesy of Professor Russell Mesler).

flattens against the receiving liquid, this would occur over a time of the order a/U, with a corresponding acceleration of the order U^2/a which, for the experimental conditions of Carroll & Mesler, is about 2000 m/s^2 and therefore smaller by an order of magnitude than the one needed for the Rayleigh–Taylor mechanism to be effective. These considerations suggest that the explanation given in the present paper is more plausible than that based on the Rayleigh–Taylor instability, but experiments will be needed for a firmer conclusion.

We wish to thank Professor Michael Longuet-Higgins for kindly commenting on a first draft of this paper and Professor Russell Mesler for his illuminating comments and for granting us permission to reproduce one of his photographs and a drawing in figure 20. This study has been supported by the Underwater Acoustics Division of the Office of Naval Research.

REFERENCES

BAKER, G. R., MEIRON, D. I. & ORSZAG, S. A. 1982 Generalized vortex methods for free-surface flow problems. *J. Fluid Mech.* **123**, 477–501.

BAKER, G. R., MEIRON, D. I. & ORSZAG, S. A. 1984 Boundary integral methods for axi-symmetric and three-dimensional Rayleigh–Taylor instability problems. *Physica* **12D**, 19–31.

BATCHELOR, G. K. 1967 *An Introduction to Fluid Dynamics*. Cambridge University Press.

BERGMAN, T. & MESLER, R. 1981 Bubble nucleation studies Part I: Formation of bubble nuclei in superheated water by bursting bubbles. *AIChE J.* **27**, 851.

BIRKHOFF, G. 1954 Note on Taylor instability. *Q. Appl. Maths* **12**, 306–309.

BLANCHARD, D. C. & WOODCOCK, A. H. 1957 Bubble formation and modification in the sea and its meteorological significance. *Tellus* **9**, 145–158.

CARROLL, K. & MESLER, R. 1981 Bubble nucleation studies. Part II: Bubble entrainment by drop-formed vortex rings. *AIChE J.* **27**, 853–856.

CHANDRASEKHAR 1961 *Hydrodynamic and Hydromagnetic Stability*. Oxford University Press (reprinted by Dover, 1981).

CHAPMAN, D. S. & CRITCHLOW, P. R. 1967 Formation of vortex rings from falling drops. *J. Fluid Mech.* **29**, 177–185.

DINGLE, A. N. & LEE, Y. 1972 Terminal fallspeeds of raindrops. *J. Appl. Met.* **11**, 877–879.

EPSTEIN, P. S. & PLESSET, M. S. 1950 On the stability of gas bubbles in liquid–gas solutions. *J. Chem. Phys.* **18**, 1505–1509.

ESMAILIZADEH, L. & MESLER, R. 1986 Bubble entrainment with drops. *J. Colloid Interface Sci.* **110**, 561–574.

FRANZ, G. J. 1959 Splashes as sources of sound in liquids. *J. Acoust. Soc. Am.* **31**, 1080–1096.

HARLOW, F. H. & SHANNON, J. P. 1967*a* The splash of a liquid drop. *J. Appl. Phys.* **38**, 3855–3866.

HARLOW, F. H. & SHANNON, J. P. 1967*b* Distortion of a splashing liquid drop. *Science* **157**, 547–550.

JASWON, M. A. & SYMM, G. T. 1977 *Integral Equation Methods in Potential Theory and Elastostatics*. Academic.

KELLER, J. B. & MIKSIS, M. J. 1983 Surface tension driven flows. *SIAM J. Appl. Maths* **43**, 268–277.

KOROBKIN, I. I. & PUKHNACHOV, V. V. 1988 Initial stage of water impact. *Ann. Rev. Fluid Mech.* **20**, 159–185.

LUNDGREN, T. S. & MANSOUR, N. N. 1988 Oscillations of drops in zero gravity with weak viscous effects. *J. Fluid Mech.* **194**, 479–510.

NYSTUEN, J. A. 1986 Rainfall measurements using underwater ambient noise. *J. Acoust. Soc. Am.* **79**, 972–982.

NYSTUEN, J. A. & FARMER, D. M. 1988 The sound generated by precipitation striking the ocean surface. In *Natural Mechanisms of Surface-Generated Noise in the Ocean* (ed. B. R. Kerman), pp. 485–499. Reidel.

OGUZ, H. N. 1989 Free surface potential flows with surface tension. *J. Comp. Phys.* (to be submitted).

PLESSET, M. S. 1954 On the stability of fluid flows with spherical symmetry. *J. Appl. Phys.* **25**, 96–98.

PROSPERETTI, A., PUMPHREY, H. C. & CRUM, L. A. 1989 The underwater noise of rain. *J. Geophys. Res.* (in press).

PUMPHREY, H. C. & CRUM, L. A. 1988 Acoustic emissions associated with drop impacts. In *Natural Mechanisms of Surface-Generated Noise in the Ocean* (ed. B. R. Kerman), pp. 463–483. Reidel.

PUMPHREY, H. C., CRUM, L. A. & BJORNO, L. 1989 Underwater sound produced by individual drop impacts and rainfall. *J. Acoust. Soc. Am.* (in press).

RODRIGUEZ, F. & MESLER, R. 1988 The penetration of drop-formed vortex rings into pools of liquid. *J. Colloid Interface Sci.* **121**, 121–129.

ROGERS, W. B. 1858 On the formation of rotating rings by air and liquids under certain conditions of discharge. *Am. J. Sci. Arts, Second Series* **26**, 246.

TAYLOR, G. I. 1959 The dynamics of thin sheets of fluid. III. Disintegration of fluid sheets. *Proc. R. Soc. Lond.* A**253**, 313–321.

TAYLOR, G. I. & MICHAEL, D. H. 1973 On making holes in a sheet of fluid. *J. Fluid Mech.* **58**, 625–667.

THOMSON, J. J. & NEWALL, H. F. 1885 On the formation of vortex rings by drops falling into liquids and some allied phenomena. *Proc. R. Soc. Lond.* **39**, 417.

WORTHINGTON, A. M. 1908 *A Study of Splashes.* New York: Longmans, Green, and Co.